Vision-Based Monitoring and Control for 3D Printing Process with Dynamic ROI and Path Modification Algorithm

Shinichi Ishikawa *, Takahito Yamashita, and Ryosuke Tasaki

Department of Mechanical Engineering, Aoyama Gakuin University, Sagamihara, Japan;
Email: yamashita@me.aoyama.ac.jp (T.Y.), tasaki@me.aoyama.ac.jp (R.T.)
*Correspondence: c5621134@aoyama.jp (S.I.)

***Abstract*—Additive manufacturing of Fused Deposition Modeling (FDM) type 3D printing has rapidly developed. In deposition-based layering process, errors in the lower layers are fatal defects, leading to loss of time and materials. In this study, we propose a motion control method that suppresses failures during the modeling process by using visual feedback control with an RGB camera. A camera set up near the nozzle detects the molding line and generates a new path from the coordinates obtained by the image, allowing for real-time path modification. In this paper, we conducted experiments to investigate the effect of the path modification by the calculation algorithm and the effectiveness of changes in the Region of Interest (ROI) for path modification. Experiments using stacked materials showed that the proposed method is effective in suppressing failures during the printing process by printing several layers. The proposed method is significantly different from conventional control methods in that it detects path changes during modeling and flexibly changes the path in real-time. This vision-based compensation system is expected to contribute to the automation and quality improvement of the additive manufacturing process.**

***Keywords*—3D printing, visual feedback, path planning**

I. Introduction

Additive manufacturing is a modeling process to be able to produce complex shapes without the need for molds or jigs. In recent years, the technology has been studied in a wide range of research fields, including large-scale 3D printing [1] for building structures and food 3D printing [2], which is increasingly needed for nursing food and space food due to its ability to express a variety of textures and tastes.

However, most of the conventional molding methods are based on feed-forward control based on a pre-defined path and do not provide path compensation or adoptive response to disturbances during the molding process. In the deposition-based additive manufacturing process, in which the stacked surfaces are stacked from the bottom layer up, a molding error in the bottom layer can affect subsequent layers and become a fatal defect that affects the quality of the entire product. Failure of modeling leads to a significant loss of time and materials, particularly in large-scale 3D printing processes. Therefore, a system that detects and corrects defects in real-time is needed.

Piovarci *et al.* [3] proposed a modeling method that uses reinforcement learning to modify the motion and performs suitable dispensing motion for materials with different flow properties. Another method [4] uses an AI-based vision system to identify threading, one of the defects associated with additive manufacturing. Other studies proposed defect detection methods using camera-based image processing and neural networks [5–9]. However, these methods require reference and training data in advance and require the use of materials each time. Therefore, when the scale of modeling is large, stacked modeling and AI-based detection methods are incompatible, and real-time modification during the modeling process is desirable. In this study, we extend these approaches and propose a motion planning system that detects defects during the modeling process and modifies the printing motion in real-time. In this study, we extend these approaches and propose a motion planning system that detects defects during the modeling process and modifies the printing motion in real-time. In research to perform repair operations on defects, there are methods to detect cracks in foundations using image processing and sealing [10] and methods to stack materials on objects with unknown uneven surfaces using a 3D scanner [11]. In the modeling method by Zhang *et al*. [12], a drone equipped with an RGB-D camera is used to measure 3D shapes during modeling. In addition, compensation operation is performed by position feedback to achieve high accuracy modeling. However, an approach to path modification based on the acquired 3D geometry were not used. A research group by Huang *et al*. [13, 14] has proposed a high-speed and high-precision positioning method based on high-speed vision-based motion control. This innovative work enables high-precision trajectory tracing technology for tasks such as welding and assembly. By introducing such conventional path generation methods based on visual feedback to additive manufacturing, flexible path generation is possible.

Manuscript received February 2, 2023; revised March 10, 2023; accepted March 30, 2023; published December 26, 2023.

By introducing the conventional path generation method using visual feedback to additive manufacturing, it is possible to generate paths that flexibly respond to defects that occur during the modeling process.

In this study, we introduce visual measurement using an RGB camera to solve the problem that conventional additive manufacturing technology cannot prevent failures in the manufacturing process. Real-time path planning using visual feedback enables path modification during operation. Most of the conventional methods only detect defects or mainly use AI-based path generation for path modification. The proposed method is significantly different from conventional control methods in that it detects path changes during the modeling process and flexibly modifies the print path in real-time. This real-time modification technique is superior to conventional methods for the additive manufacturing method, which consumes a large amount of material. This study aims to realize a motion-controlled "failure-free" additive manufacturing technology.

II. Hardware Apparatus

We developed a 3D printing apparatus for large-scale modeling consisting of *XYZ* axes. Fig. 1 shows the appearance of the apparatus. The molding machine consists of a gantry-type *YZ*-axis actuator and two *X*-axis actuators installed in parallel. A module for feeding material and an RGB camera (30 fps) for detecting the path is installed at the tip of the *Z*-axis actuator. The platform for molding is 1200 mm × 1000 mm in size. In the material feeding module, a stepping motor pushes a piston to dispense material from a syringe.

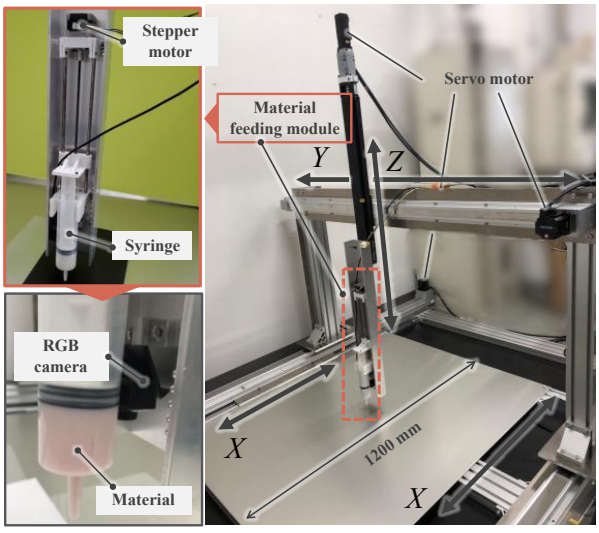

Figure 1. 3D printing apparatus consist of XYZ actuators, a RGB camera, and material feeding module.

Bingham fluid is used for the dispensing material, which is made by mixing PTFE powder at 45 wt% with silicone oil.

III. Dynamic Path Modification System

A. System Design of Vision-Based Control

Fig. 2 shows an overall illustration of the modeling system based on visual measurement. The developed 3D printing apparatus has degree of freedom and consists of a material feeding module and RBG camera for visual feedback. The camera installed at the front of dispensing nozzle observes the one layer before the printed line. The visual measurement system extracts feature points from the acquired images by image processing. The controller receives feedback from the coordinates obtained by the visual measurement system and generates motion commands for path generation in real-time.

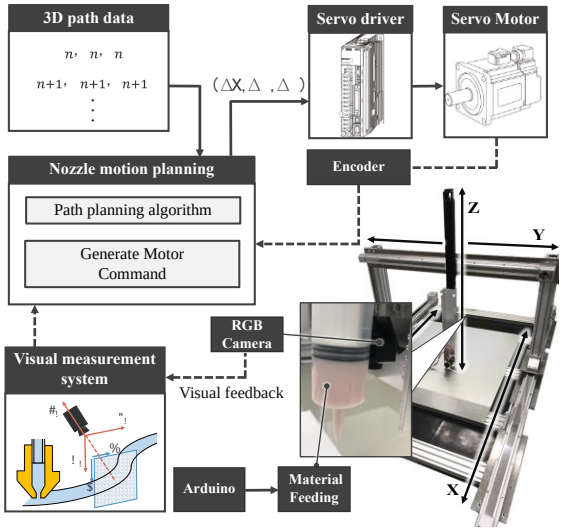

Figure 2. Dynamic control system with visual feedback.

$$\begin{bmatrix} X_w \\ Y_w \\ Z_w \\ 1 \end{bmatrix} = \begin{bmatrix} \mathbb{R} & \mathbb{T} \\ 0 & 1 \end{bmatrix} \begin{bmatrix} u \\ v \\ -f \\ 1 \end{bmatrix} = \begin{bmatrix} 1 & 0 & 0 & T_x \\ 0 & 1 & 0 & T_y \\ 0 & 0 & 1 & T_z \\ 0 & 0 & 0 & 1 \end{bmatrix} \begin{bmatrix} u \\ v \\ -f \\ 1 \end{bmatrix} \quad (1)$$

(X_w, Y_w, Z_w) are the coordinates of the measurement point in world coordinates, (u, v) are the coordinates of the measurement point in 2D coordinates. f is the focal length, which generally corresponds to the distance between the camera and the measurement plane. In this study, because the direction opposite to the measurement plane is the positive direction of the camera coordinate system (X_c, Y_c, Z_c), the distance between the camera and the stacking plane is defined as $-f$.

The coordinate transformation is based on the pinhole camera model [15] shown in Eq. (1). $\boldsymbol{R}$ and $\boldsymbol{T}$ are the rotation and translation matrices, which indicate the positional relationship between the world coordinate system and the camera coordinate system. By setting the camera coordinate system parallel to the world coordinate system, only the translation component can be used.

B. Path Planning Algorithm

Fig. 2 shows a schematic diagram of the path generation method. Here, the nozzle displacement ΔY is expressed as in Eq. (2).

$$\Delta Y = y_{n+1} + F(y_c - y_{n+1}) - y_n \quad (2)$$

$y_n, y_{(n+1)}, \ldots$ are the original motion paths obtained from the 3D shape data, and y_c is the coordinate obtained from the camera detection of the lower molding line as shown in Fig. 3. F ($0 \leq F \leq 1$)is the path compensation coefficient, which determines the strength of the compensation. In case of the coefficient of F is small, the compensation works weakly and passes close to the original motion path, which is effective when the original shape is to be retained. On the other hand, when the value of F is large, the compensation works strongly, and the path acquired by the camera is prioritized. Therefore, it is effective when the priority is on simple geometry and no failure. Thus, the route compensation coefficients can be set according to the intended use, allowing for flexible path generation. Fig. 4 shows an example of path generation based on the path generation algorithm for a sine-shaped disturbance. As shown in Fig. 4, for small values of F, the effect of the disturbance is small and the path converges to the original path quickly; for larger values of F, the path converges smoothly to the original path; for F = 1, the path follows the disturbance to follow the underlying modeling line.

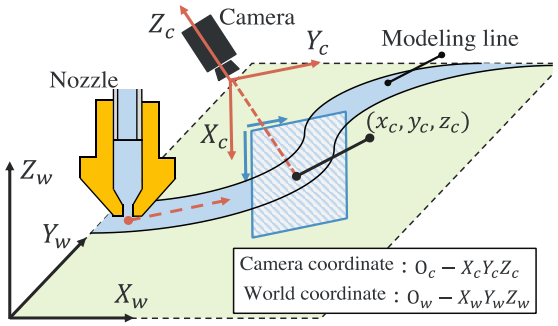

Figure 3. Path planning method.

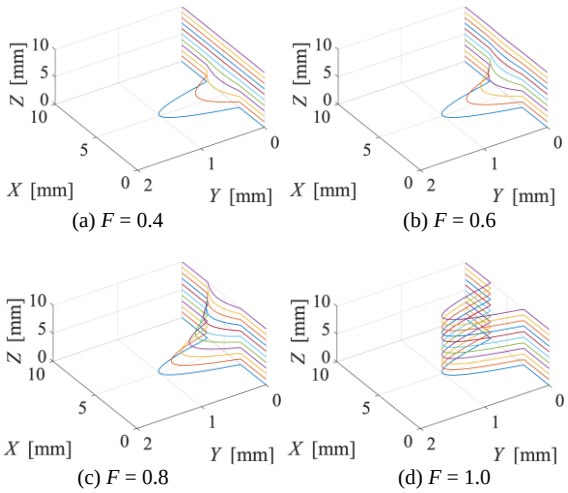

Figure 4. Print trajectory depending on coefficient F.

C. Image Processing Method

Fig. 5 shows the image processing flow. The acquired image is binarized, and the contours are extracted from the resulting binarized image. Next, a Bounding Box, which approximates the object to the smallest rectangle, is generated from the extracted contour, and its center point is extracted as a feature point. In addition, by narrowing down the target area through image processing, it is possible to generate a Bounding Box in a desired area. Based on the coordinates of the center of the Bounding Box and the path information obtained from the 3D geometry, a new path generation algorithm is used to generate a new path in real-time.

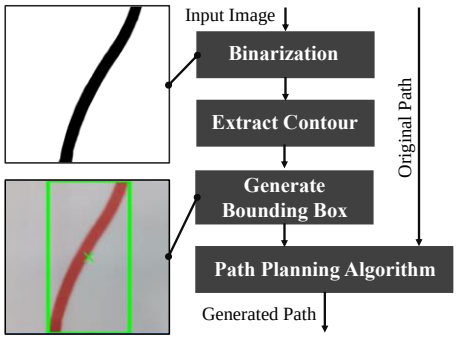

Figure 5. Flow of image processing.

IV. Evaluation for Path Modification

In this chapter, we describe the experiment to verify the tracking performance of a line that imitates a modeling line. In this chapter, we describe the experiment to verify the tracking performance of a line that imitates a modeling line, using the algorithm presented in Section III, to check the effects of compensation coefficients and changes in the Region of Interest (ROI), and the tracking performance against disturbance.

A. Experimental Equipment and Experimental Conditions

Fig. 6 shows the appearance of the apparatus used in this experiment. The RGB camera is placed 70 mm above the modeling line and observes an area of 45 mm × 80 mm (720 pixel × 1280 pixel).

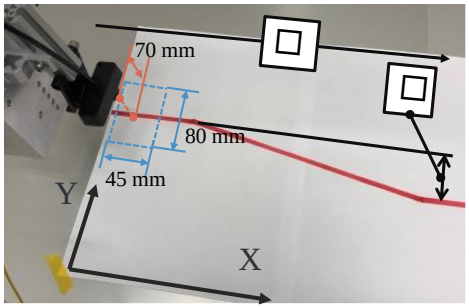

Figure 6. Nozzle mounted RGB camera and its observed area.

In the experiment, the X-axis is fed at a constant speed v [mm/s] while the Y-axis is moved to compensate for the

path. A pre-printed line with a width of 5 mm was prepared as the base for the modeling and was used for detection. Experiments were conducted at different feed speeds and linear shapes as shown in Table I. The experiments were conducted to compare the tracking performance with the compensation coefficient F, to investigate the effect of compensation for dynamic disturbances, and to investigate the effect of changes in the ROI on the path change.

TABLE I. MODELING PARAMETER

Parameters	Value
Index of Flexibility F [-]	0.5, 0.8, 1.0
Travel Speed v [mm/s]	9.6, 19.2
Displacement L [mm]	60, 120
Line width w [mm]	5

B. Evaluation of Tracking Performance

The RMSE [mm] (Root Mean Square Error) and maximum error [mm] were calculated from the paths obtained from the experimental results for each condition and the path to be tracked.

The RMSE and maximum error for each condition is shown in Fig. 7. Fig. 8 shows an example of experimental results for L = 60, F = 1.0, and v = 8.6. The experimental results show that the error tends to increase as the value of the path compensation coefficient F increases. As shown in Eq. (1), the smaller the value of F, the smaller the compensation by the camera, and the more the original print path is referenced, thus confirming the validity of the compensation effect. No significant differences were observed with changes in speed. The maximum error for L = 60 was within the range of the line width: 5 mm, but for L = 120, the error was larger than the line width. These results suggest that it is necessary to determine the appropriate compensation coefficients according to the 3D geometry data and the purpose of use.

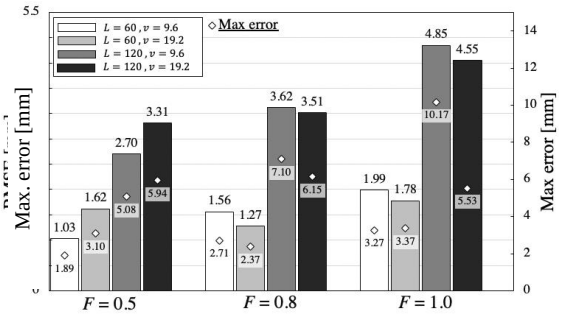

Figure 7. Experimental result of RMSE of in each condition.

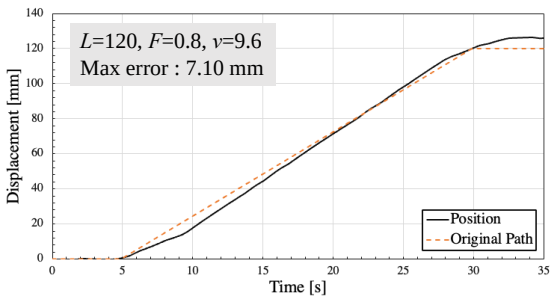

Figure 8. Displacement of Y axis.

C. Verification of Modification Effect against Disturbance

To confirm the effect of compensation for dynamic disturbance, a disturbance of about 20 mm was applied to the base in the Y-axis direction by hand (at t = 11 s) under the conditions of L = 60, F = 1.0, and v = 9.6, and then the base was moved back to its original position (at t = 20 s).

The results of the experiment and the compensation during the experiment are shown in Figs. 9 and 10. The experimental results show that there is some overshoot after path modification, but it converges in about 1 s, which is considered sufficient in terms of adaptation to additive manufacturing. Thus, it can be confirmed that the path is compensated in real-time by using the camera to provide feedback on the path changes caused by the disturbance.

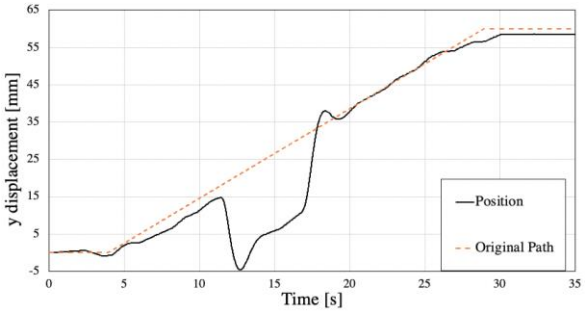

Figure 9. Line tracking experiment with disturbance.

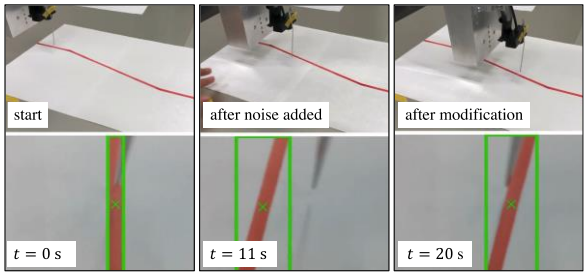

Figure 10. Time-lapse of the experiment.

D. Changes of Path Generation in Dynamic Region of Interest (ROI)

Experiments have been conducted with different sizes of ROI and different path changes, for a total of eight patterns. Bounding Box for a small ROI was generated by removing 1/4 of the observation area (left and right) and 1/3 of the observation area (top and bottom). Four patterns of angular changes in the path were prepared, ranging from 45° to 75° in 10° increments.

Figs. 11 and 12 show the amount of compensation in the Y-axis direction for each condition, with the dashed line representing the trajectory of the target line and the solid line representing the trajectory drawn by the apparatus.

The results for each condition showed that the smaller the ROI, the smaller the error from the actual trajectory at the corner of the target line, and the larger the ROI, the more the motion tends to take a shortcut-like motion path.

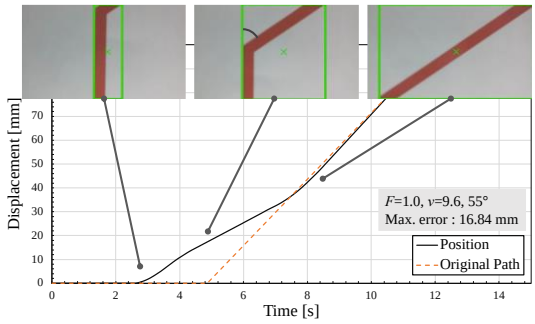

(a) large size of Bounding Box (corner angle: θ is 55°)

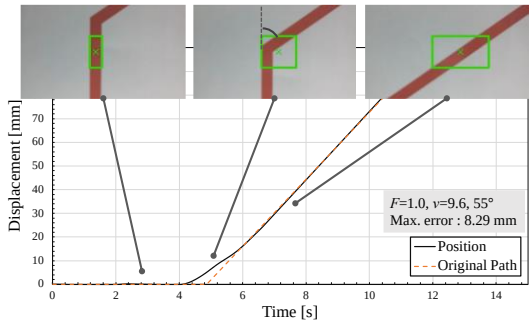

(b) small size of Bounding Box (corner angle: θ is 55°)

Figure 11. Comparative results for different size of ROI.

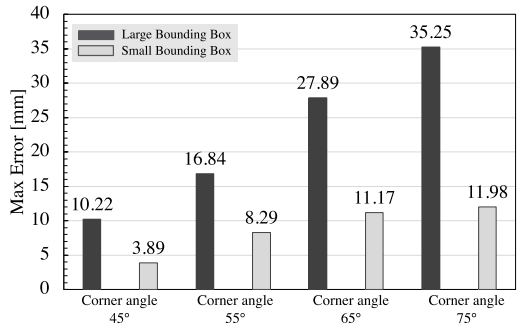

Figure 12. Maximum error in each condition.

The maximum error [mm] for each condition is shown in Fig. 12. The results show that the maximum error is reduced by about 60% by reducing the observation area. In addition, the larger the angle change, the larger the deviation at the corners, with a maximum deviation of 35.25 mm at an angle change of 75°. Therefore, as the angle change increases, it is easy to lose sight of the target line as it deviates from the observation area of the camera. While the deviation can be suppressed by decreasing the observation area, the deviation from the observation area causes the camera to deviate from the target line and lose sight of the detected target line.

Based on the results of the experiment, we constructed an algorithm that automatically changes the ROI according to the angle of the path.

In this algorithm, when the angle change of the path is small, the ROI is set to be large to increase stability. When the angle change is large, the ROI is set to be small to suppress the error. In this way, the observation area is set according to the angle change. The angle changes are calculated from the three points obtained from the upper, middle, and lower sections of the path.

Fig. 13 shows the results of ROI generation obtained by this algorithm. The path generation results show that it is possible to set ROIs according to the path changes.

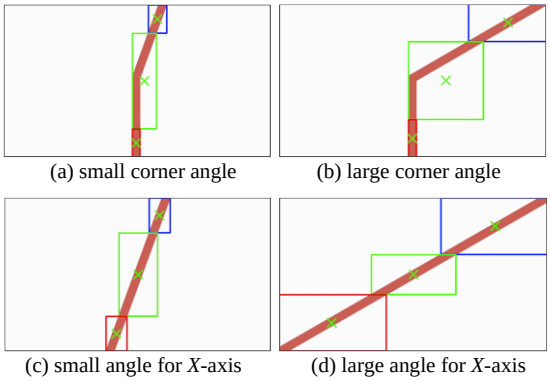

(a) small corner angle (b) large corner angle

(c) small angle for *X*-axis (d) large angle for *X*-axis

Figure 13. Generation of dynamic ROI.

V. Path Modification Experiment Experiment

In this chapter, we describe modeling experiments using storable materials to demonstrate the effectiveness of the path modification system as shown in Section III.

A. Expereimental Condition

Several experiments on path compensation using stackable materials have been conducted. The trial material is a Bingham fluid made by mixing silicon oil and PTFE powder. The camera is mounted 35 mm in front of the nozzle, and the time delay is applied according to the offset distance between the camera and the nozzle so that the nozzle can follow the line of the modeling line. Nozzle feed velocity is v = 9.6 mm/s.

To form layered material, three layers of straight lines are formed, and then a jig with a radius of 50 mm created by a 3D printer is used to reproduce the shape changes in anticipation of errors during the forming process. The modeling line created in this way is used as the target for three additional layers of modeling with compensation for the path using a camera. In this way, a compensation path generation was performed by visual feedback to demonstrate the effectiveness of the compensation effect.

B. Result and Discussion

Fig. 14 shows the appearance of the specimen obtained from the experiment. The experimental results show that when no compensation is performed by the camera (Fig. 14(a)), the operation is performed regardless of the change in shape, and it can be confirmed that the specimen is not formed correctly. However, when compensation is performed by the camera (Fig. 15(b)), the camera feedback changes in the shape and modifies the path, so that molding is performed without collapsing.

Fig. 15 shows the amount of compensation for the Y-axis when the camera is used to compensate for the 4–6 layers. Fig. 16 shows the fifth layer and the detection of the molding line by the camera. The results in Fig. 15 show that the path tends to be more inner than that of the lower layers as the layers are added at around 6–8 s. As shown in Fig. 16(b) and the lower part of Fig. 16(d), this may be

because the generated Bounding Box detects not only the lines of the lower layer but also those of the previous layers, resulting in a larger than expected size. It can also be confirmed that the generated path is larger than the actual path at around 9 s in Fig. 15. This may be due to temporarily excessive coordinates being acquired due to inaccurate detection of the modeling lines. To solve this problem, we will improve the detection accuracy by adjusting the numerical parameters during binarization and by adjusting the illumination.

(a) with visual feedback (b) without visual feedback

Figure 14. Layered material obtained from experiment.

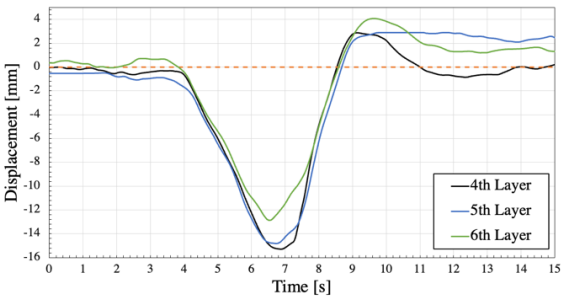

Figure 15. Displacement of *Y* axis.

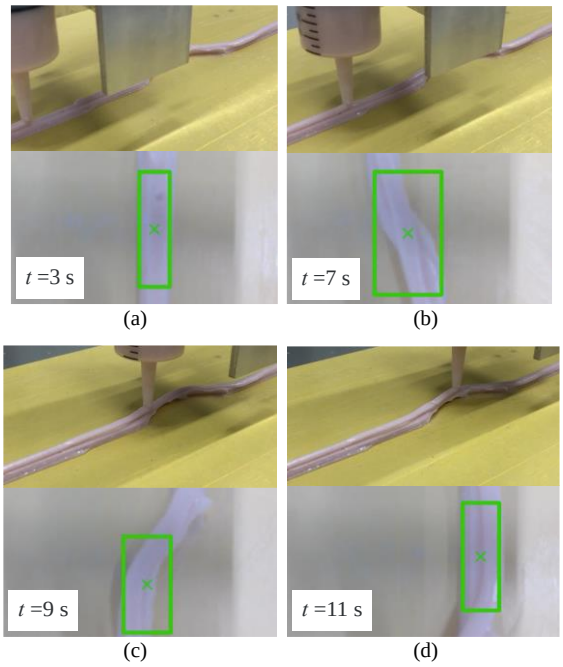

(a) (b) (c) (d)

Figure 16. Time-lapse of in 5th layer.

The fundamental effectiveness of real-time visual-based path modification in the additive manufacturing process is demonstrated. For practical use, it is necessary to introduce a camera-based detection algorithm for a practical environment and necessary to improve the modeling accuracy.

VI. Conclusion

We proposed a path modification method using visual measurement with an RGB camera as an approach to suppress failures during modeling process. In the path planning algorithm, modification paths are newly generated according to the predetermined value of the compensation coefficient *F*. In this paper, we evaluated the validity of the path generation method and its tracking ability by experiments on lines that imitate modeling lines. In addition, the effect of the change of the Region of Interest (ROI) by the RGB camera on the path generation is discussed.

In addition, the effect of modification on molding defects was verified using materials that were assumed to be stacked. A total of six layers are formed, and the path modification experiments confirmed the modification effect of the RGB camera on path changes during molding, which suppressed modeling failures.

This vision-based modeling method is expected to be used for architectural 3D printing, where modeling failures have a large impact. In the near future, 3D measurement and 3D motion control of the modeling line will be performed using an RGB-D camera.

Conflict of Interest

The authors declare no conflict of interest.

Author Contributions

S. Ishikawa conducted all experiments and analyzed data. T. Yamashita supervised the setup of each experiment and the designing of the experimental apparatus. All research activities were conducted under the supervision and coordination of R. Tasaki. All authors contributed to the writing of the paper and approved its final version.

References

[1] X. Zhang, M. Li, J. H. Lim, Y. Weng, Y. W. D. Tay, H. Pham, and Q.-C. Pham, "Large-scale 3D printing by a team of mobile robots," *Automation in Construction*, vol. 95, pp. 98–106, 2018.

[2] S. Mantihal, S. Prakash, F. C. Godoi, and B. Bhandari, "Optimization of chocolate 3D printing by correlating thermal and flow properties with 3D structure modeling," *Innovative Food Science and Emerging Technologies*, vol. 44, pp. 21–29, 2017.

[3] M. Piovarci, M. Foshey, J. Xu, T. Erps, V. Babaei, P. Didyk, S. Rusinkiewicz, W. Matusik, and B. Bickel, "Closed-loop control of direct ink writing via reinforcement learning," *ACM Trans. Graph*, vol. 41, no. 4, pp. 1–5, 2022.

[4] K. Paraskevoudis, P. Karayannis, and E. P. Koumoulos, "Real-time 3D printing remote defect detection (stringing) with computer vision and artificial intelligence," *Processes*, vol. 8, no. 1464, pp. 1–15, 2020.

[5] D. A. J. Brion and S. W. Pattinson, "Generalisable 3D printing error detection and correction via multi-head neural networks," *Nature Communications*, vol. 13, no. 4654, pp. 1–14, 2022.

[6] T. Huang, S. Wang, S. Yang, and W. Dai, "Statistical process monitoring in a specified period for the image data of fused deposition modeling parts with consistent layers," *Journal of Intelligent Manufacturing*, vol. 32, pp. 2181–2196, 2021.

[7] J. Liao, Z. Shen, G. Xiong, C. Liu, C. Luo, and J. Lu, "Preliminary study on fault diagnosis and intelligent learning of Fused Deposition Modeling (FDM) 3D printer," in *Proc. 14th IEEE Conference on Industrial Electronics and Applications (ICIEA)*, 2019, pp. 2098–2102.

[8] Y. Fu, A. Downey, L. Yuan, A. Pratt, and Y. Balogun, "In situ monitoring for fused filament fabrication process: A review," *Additive Manufacturing*, vol. 38, 101749, 2021.
[9] J. Fastowicz, M. Grudziński, M. Tecław, and K. Okarma, "Objective 3D printed surface quality assessment based on entropy of depth maps," *Entropy*, vol. 21, no. 97, 2019.
[10] J. Liu, X. Yang, X. Wang, and J. W. Yam, "A laboratory prototype of automatic pavement crack sealing based on a modified 3D printer," *International Journal of Pavement Engineering*, vol. 23, pp. 1–12, 2022.
[11] N. Bausch, D. P. Dawkins, R. Frei, and S. Klein, "3D printing onto unknown uneven surfaces," *IFAC-PaperOnLine*, vol. 49, no. 21, pp. 583–590, 2016.
[12] K. Zhang, P. Chermprayong, F. Xiao, D. Tzoumanikas *et al*., "Aerial additive manufacturing with multiple autonomous robots," *Nature*, vol. 609, pp. 709–717, 2022.
[13] S. Huang, Y. Yamakawa, T. Senoo, and M. Ishikawa, "Realizing 1D robotic catching without prediction based on dynamic compensation concept," in *Proc. International Conference on Advanced Intelligent Mechatronics*, 2015, pp. 1629–1634.
[14] S. Huang, Y. Yamakawa, T. Senoo, and M. Ishikawa, "Dynamic compensation by fusing a high-speed actuator and high-speed visual feedback with its application to fast peg-and-hole alignment," *Advanced Robotics*, vol. 28, no. 9, pp. 613–624, 2014.
[15] I. Carlbom and J. Paciorek, "Planar geometric projections and viewing transformations," *ACM Computing Surveys*, vol. 10, no. 4, pp. 465–502, 1978.